The Journal of Chemical Physics

A computational study of electrolyte adsorption in a simple model for intercalated clays

Cite as: J. Chem. Phys. **132**, 104705 (2010); https://doi.org/10.1063/1.3357351
Submitted: 13 October 2009 . Accepted: 17 February 2010 . Published Online: 10 March 2010

E. Lomba, and J.-J. Weis

A computational study of electrolyte adsorption in a simple model for intercalated clays

E. Lomba[1,a)] and J.-J. Weis[2]
[1]*Instituto de Química-Física Rocasolano, CSIC, Serrano 119, E-28006 Madrid, Spain*
[2]*Laboratoire de Physique Théorique, Université Paris-Sud, UMR 8627, Bâtiment 210, 91405 Orsay Cedex, France*

(Received 13 October 2009; accepted 17 February 2010; published online 10 March 2010)

A pillared interlayered clay is represented by a two-dimensional quenched charged disordered medium, in which the pillar configuration is produced by the quench of a two-dimensional electrolyte and the subsequent removal of the anions (that act as a template). The cation charge is counterbalanced by a neutralizing background that is an ideal representation of the layer's negative charge in the experimental system. In this paper we investigate the adsorption of electrolyte particles in this charged disordered medium resorting both to the use of the replica Ornstein–Zernike equation in the hypernetted chain approximation and grand canonical Monte Carlo simulations. The theoretical approach qualitatively reproduces the simulated behavior of the adsorbed fluids. Theoretical estimates of the material porosities obtained for various types of pillar distributions are in good agreement with the simulation. We investigate the influence of the matrix on correlation functions and adsorption isotherms. © *2010 American Institute of Physics*. [doi:10.1063/1.3357351]

I. INTRODUCTION

Intercalated clays [or pillared interlayered clays (PILCs)] have been shown to possess a great technological potential for gas separation processes and in catalysis.[1,2] These materials are synthesized by cation exchange in a cationic clay from the smectite group[3] and subsequent calcination, by which pillars are introduced between the layers of the original layered structure. In this way, a layered structure with fixed interlayer distance is constructed, with the practical advantage that the interlayer separation can be tuned at will by choosing the appropriate pillaring agent. Thus, one can design adsorbents[4] with geometries ranging from pure quasi-two-dimensional porous materials to periodic layered systems with interlayer separations up to 2 nm. These systems, although exhibiting periodicity along one spatial dimension (orthogonal to the layers), are characterized by the absence of long-range order in the distribution of pillars. In fact, being this property directly influenced by the process of synthesis, and given that the parent clays are natural products with a certain degree of randomness in the position of some of their constituent cations, the problem of a quantitative characterization of the pillar distribution is far from settled. It is nonetheless clear that a statistical description will be needed to characterize these systems.

A theoretical modeling of this type of materials is rather challenging. In principle, they can be cast into the class of partly quenched systems, given the fact that the precise location of the pillars is unknown and that one can have many pillar configurations in the same microcrystalline sample (and possibly there are few correlations between the pillars of adjacent layers). Moreover, the process of synthesis, in which the pillars are inserted within the layer structure (cation exchange and calcination to remove the solvent), has some resemblance with the templating process that is a well established procedure for the synthesis of porous materials.[5,6] These features suggest that the replica Ornstein–Zernike (ROZ) theory, first proposed by Madden and Glandt[7] and later properly reformulated by Given and Stell,[8] could be a feasible approach to tackle this problem, in particular, since Zhang and Van Tassel[9] showed that the ROZ equations can also be used to describe templated porous materials, in which one (or various) of the components that build the matrix is removed after the quenching process. Closely connected to these systems are the spongelike materials for which Zhao *et al.*[10,11] also recently formulated the ROZ equations. It is then tempting to try out the capabilities of the ROZ approach to model the adsorption process in a system with some resemblance to a cationic intercalated clay. In the case that the interlayer distance is larger than a few molecular diameters, the problem posed is rather involved, and is related to the inhomogeneous partly quenched systems for which Pizio and Sokolowski[12] solved the computationally demanding inhomogeneous ROZ equation. A much simpler Fisher–Methfessel approximation was used by Pérez *et al.*[13] in combination with a Born–Green–Yvon equation in order to describe capillary condensation in a slitlike pore filled with quenched disorder. On the other hand, in the limit of interlayer distance approaching one molecular diameter, we are back to a purely two-dimensional system, in which the disordered matrix is formed by a quenched distribution of cations [interacting via three-dimensional (3D) Coulombic interactions] constrained to lie on a plane by the two clay layers. Charge neutrality is enforced by the negative charges more or less randomly distributed all over the layers. This

a)Electronic mail: e.lomba@iqfr.csic.es.

problem can be cast into a form amenable to be straightforwardly solved in terms of the templated ROZ approach in two dimensions.

The aim of this paper is then to investigate the ability of the ROZ theory to describe a simple two-dimensional model for an intercalated clay, and to explore the properties of this model system, using ROZ equations and Monte Carlo (MC) simulations, both in the canonical and grand canonical MC (GCMC) ensemble. We will be dealing with a partly quenched system, in which the porous media (adsorbent or porous matrix) will be constructed by quenching an electrolyte [a neutral mixture of charged hard spheres (HS)] constrained to lie within a surface (which models the interlayer space), and subsequent removal of the negative ions (which play the role of template). The negative charge of the layers is incorporated in the model as a continuous background so that our porous system can be treated on the same footing as a quenched plasma.[14] This rather simplistic approach can be justified as follows. A standard cationic clay of the smectite group, such as montmorillonite,[3] is formed by stacking of layers with 0.98–1.98 nm thickness, each of them formed by an octahedral layer sandwiched between two SiO_4 tetrahedral layers. The octahedral layer contains Al^{3+} cations, some of which ($\approx 1/8$) are substituted by Mg^{2+}, and this generates an excess of negative charge in the layers. This excess is counterbalanced by hydration cations in the parent clay and by the pillars in the final PILC. In a natural product, such as these clays, the distribution of negative charges is far from being completely uniform. Since this excess of negative charge emanates from the substitution Mg^{2+} cations that are well buried inside a rather thick layer, it appears reasonable that a two-dimensional representation of the interlayer space, which we intend to model, could account for the layer's negative excess charge by means of a neutralizing background. This will counterbalance the positive charge of the cationic pillars. If we were to deal with a fully 3D model, the layer charge could otherwise be distributed in point charges on the layers, according to a more or less irregular fashion, but this would lead to a substantially more complex system (and not necessarily better than our simple approach for our purposes).

As to the adsorbate (or annealed fluid) we will consider here an electrolyte modeled by charged HSs. Again in this case, we will restrict ourselves to the simplest case of the well-known primitive model, in which the solvent only enters implicitly the problem through the dielectric constant. This is obviously a very strong simplification that leaves out the explicit consideration of solvation effects. These however, can be incorporated as a first order approximation in an "effective" fashion following the old approach suggested by Debye and Hückel.[15] The extended Debye–Hückel theory, which incorporates the ion size explicitly, can be brought to a considerable better agreement with the experimental results if the value of the ionic radii is assumed to be substantially larger than the typical crystallographic radii. This can be interpreted in the sense that the effective size of the ion in solution represents in fact that of the hydrated ion. In this way, treating the ion diameters as adjustable parameters, one can effectively incorporate, to a certain extent, some of the effects of hydration. It is to be recognized that this is a standard preliminary step in any statistical mechanical approach to model ionic solutions, and the explicit treatment of the solvent, although computationally more involved is feasible.[16,17] For the purpose of this paper, however, we believe that the primitive level approach (in which the solvent enters the problem effectively through the dielectric constant and adjustable ionic sizes) should be sufficient.

Under these constraints, we will investigate the adsorption of symmetric and asymmetric electrolytes in various matrix topologies by means of ROZ integral equations in the hypernetted chain (HNC) approximation and by computer simulation. Our system is related to those that have been used to model electrolyte adsorption in charged matrices,[18–20] with the exception that in our case one of the matrix constituents acts as a template and is removed after quenching.

The rest of the paper is organized as follows. In Sec. II we introduce the details of our model and summarize the key equations of the ROZ-HNC theory, including thermodynamics, and we present an alternative approach to obtain theoretical estimates for the matrix porosity. Section III contains the details of the simulation approach, and finally in Sec. IV our most significant results are presented and discussed.

II. THE MODEL: REPLICA ORNSTEIN–ZERNIKE THEORY

Our model is composed of 3D charged HSs constrained to lie within a plane. We will have N_+ cations and N_- anions of charges $z_\pm$, in area A (by which the number densities will be $\rho_\pm = N_\pm / A$), satisfying the charge neutrality condition, $z_+\rho_+ + z_-\rho_- = 0$. Additionally we will have M matrix particles of positive charge z_{m_+} (in the case of a cationic clay). Our system is thus described by a Hamiltonian of the form

$$U_N(\mathbf{r}_1, \ldots, \mathbf{r}_N; \{\mathbf{R}_1, \ldots, \mathbf{R}_M\}) = \sum_{i>j} V_{\alpha\nu}(r_{ij}) + \sum_i^N \sum_j^M V_{\alpha m_+}(|\mathbf{r}_i - \mathbf{R}_j|), \tag{1}$$

where $\mathbf{r}_i$ and $\mathbf{R}_i$ describe the fluid and matrix particle positions, respectively, and the ion-ion interaction is given by (α and ν denote + or −)

$$\beta V_{\alpha\nu}(r) = \begin{cases} \infty & \text{if } r < (\sigma_\alpha + \sigma_\nu)/2 \\ z_\alpha z_\nu \Gamma / r & \text{otherwise,} \end{cases} \tag{2}$$

and the matrix-ion interactions by

$$\beta V_{\alpha m_+}(r) = \begin{cases} \infty & \text{if } r < (\sigma_\alpha + \sigma_{m_+})/2 \\ z_\alpha z_{m_+} \Gamma / r & \text{otherwise,} \end{cases} \tag{3}$$

with $\Gamma = e^2/(4\pi\epsilon\epsilon_0\sigma k_B T)$, where k_B is Boltzmann's constant, T is the absolute temperature, e is the electron charge, σ is the unit length diameter (in our case that of the smallest ion), and ϵ and ϵ_0 are the relative and vacuum permittivities, respectively. Throughout this paper thus, r will be measured in units of the smallest ion diameter, and we will define a reduced temperature by $T^* = 1/\Gamma$. Before quenching and template removal, the interaction between the matrix precursor components is given by

$$\beta V_{m_i m_j}(r) = \begin{cases} \infty & \text{if } r < (\sigma_{m_i} + \sigma_{m_j})/2 \\ z_{m_i} z_{m_j} \Gamma / r & \text{otherwise.} \end{cases} \tag{4}$$

As mentioned before, once the configurations of the matrix precursor (a $z_{m_+}:z_{m_-}$ electrolyte) are quenched, the template (m_- component) is removed.

A. ROZ equations

The ROZ equations for our model are essentially those formulated by Hribar *et al.*[18,19] for an asymmetric electrolyte adsorbed in a electroneutral matrix. The templating process only affects the matrix-fluid closure relations. Following Zhang and Van Tassel,[9] one should simply dismiss the interactions between the negative matrix particles (which are removed after quenching) and the adsorbed ionic particles. Note, however, that the correlations involving the template particles will enter the ROZ equations, and it will be possible to determine the correlation between the "holes" left by the template particles and the adsorbed fluid. In order to express the equations in a more compact fashion, we will define our two-dimensional Fourier transforms as

$$\tilde{f}_{\alpha\nu}(k) = 2\pi\sqrt{\rho_\alpha \rho_\nu} \int_0^\infty dr r f_{\alpha\nu}(r) J_0(kr) \tag{5}$$

and

$$f_{\alpha\nu}(r) = \frac{1}{2\pi\sqrt{\rho_\alpha \rho_\nu}} \int_0^\infty dk k \tilde{f}_{\alpha\nu}(k) J_0(kr), \tag{6}$$

where $J_0(x)$ is the zeroth-order Bessel function of the first kind, $f_{\alpha\nu}$ stands for any correlation function between particles of types α and ν, and ρ_λ is the number density of particles of type λ. The Bessel transforms of Eqs. (5) and (6) can be evaluated using Lado's approach, in order to guarantee (up to machine precision) the orthogonality of the forward and backward transforms,[21] or alternatively one can use Talman's method,[22] in which the logarithmic grid is particularly well suited to extremely long ranged correlations. In the present instance we have resorted to Lado's method due to its orthogonality properties. Now, the corresponding ROZ equations can be compactly written in matrix form in Fourier space as

$$\begin{aligned} \boldsymbol{H}^{01} &= \boldsymbol{C}^{01} + \boldsymbol{C}^{00}\boldsymbol{H}^{01} + \boldsymbol{C}^{01}\boldsymbol{H}^{11} - \boldsymbol{C}^{01}\boldsymbol{H}^{12}, \\ \boldsymbol{H}^{11} &= \boldsymbol{C}^{11} + \boldsymbol{C}^{10}\boldsymbol{H}^{01} + \boldsymbol{C}^{11}\boldsymbol{H}^{11} - \boldsymbol{C}^{12}\boldsymbol{H}^{12}, \\ \boldsymbol{H}^{12} &= \boldsymbol{C}^{12} + \boldsymbol{C}^{10}\boldsymbol{H}^{01} + \boldsymbol{C}^{11}\boldsymbol{H}^{12} + \boldsymbol{C}^{12}\boldsymbol{H}^{11} - 2\boldsymbol{C}^{12}\boldsymbol{H}^{12}, \end{aligned} \tag{7}$$

and the decoupled matrix equation

$$\boldsymbol{H}^{00} = \boldsymbol{C}^{00} + \boldsymbol{C}^{00}\boldsymbol{H}^{00}, \tag{8}$$

where superscripts 0 and 1 denote the matrix and the fluid, respectively, and 2 denotes the replicas of fluid particles. Now, each of the matrix functions $\boldsymbol{F}^{ij}$ (where $\boldsymbol{F}$ stands for either $\boldsymbol{H}$ or $\boldsymbol{C}$) can be explicitly expressed in terms of the density scaled Fourier transforms of the total correlation function, $\tilde{h}_{\alpha\nu}$, or direct correlation function, $\tilde{c}_{\alpha\nu}$, according to

$$\boldsymbol{F}^{01} = \begin{pmatrix} \tilde{f}_{m_+ +} & \tilde{f}_{m_+ -} \\ \tilde{f}_{m_- +} & \tilde{f}_{m_- -} \end{pmatrix}, \quad \boldsymbol{F}^{11} = \begin{pmatrix} \tilde{f}_{++} & \tilde{f}_{+-} \\ \tilde{f}_{-+} & \tilde{f}_{--} \end{pmatrix}, \tag{9}$$

$$\boldsymbol{F}^{12} = \begin{pmatrix} \tilde{f}^r_{++} & \tilde{f}^r_{+-} \\ \tilde{f}^r_{-+} & \tilde{f}^r_{--} \end{pmatrix}$$

and correspondingly for the matrix

$$\boldsymbol{F}^{00} = \begin{pmatrix} \tilde{f}_{m_+ m_-} & \tilde{f}_{m_+ m_-} \\ \tilde{f}_{m_- m_+} & \tilde{f}_{m_- m_-} \end{pmatrix}. \tag{10}$$

In the equations above, + and − represent the cations and anions of the adsorbed electrolyte, respectively, and m_+ and m_- denote the two matrix components, of which m_- is the template, and finally the superscript r denotes correlations between the replicas of the corresponding annealed ions. Additionally we have $\boldsymbol{F}^{10} = \boldsymbol{F}^{01^T}$, where the superscript T denotes the matrix transpose. These equations in the Fourier space are complemented by the corresponding closures in r-space, which in the HNC approximation read

$$\begin{aligned} h_{\alpha\nu}(r) &= \exp(-\beta V_{\alpha\nu}(r) + h_{\alpha\nu}(r) - c_{\alpha\nu}(r)) - 1, \\ h_{m_+\nu}(r) &= \exp(-\beta V_{m_+\nu}(r) + h_{m_+\nu}(r) - c_{m_+\nu}(r)) - 1, \\ h_{m_-\nu}(r) &= \exp(h_{m_-\nu}(r) - c_{m_-\nu}(r)) - 1, \\ h^r_{\alpha\nu}(r) &= \exp(h^r_{\alpha\nu}(r) - c^r_{\alpha\nu}(r)) - 1, \end{aligned} \tag{11}$$

where again, α and ν stand for the + and − adsorbed ions, and $f_{m_i\alpha} = f_{\alpha m_i}$. For the matrix, we also have

$$h_{m_i m_j}(r) = \exp(-\beta V_{m_i m_j}(r) + h_{m_i m_j}(r) - c_{m_i m_j}(r)) - 1, \tag{12}$$

where the interaction between the matrix components before the template is removed is given by Eq. (4). Equations (12) and (8) can be solved independently. As to Eq. (7), for computational convenience they can be cast into a more compact matrix form

$$\begin{pmatrix} \boldsymbol{C}^{01} \\ \boldsymbol{C}^{11} \\ \boldsymbol{C}^{12} \end{pmatrix} = \begin{pmatrix} \boldsymbol{I} - \boldsymbol{C}^{00} & -\boldsymbol{C}^{01} & \boldsymbol{C}^{01} \\ -\boldsymbol{C}^{10} & \boldsymbol{I} - \boldsymbol{C}^{11} & \boldsymbol{C}^{12} \\ -\boldsymbol{C}^{10} & -\boldsymbol{C}^{12} & \boldsymbol{I} - \boldsymbol{C}^{11} + 2\boldsymbol{C}^{12} \end{pmatrix} \begin{pmatrix} \boldsymbol{H}^{01} \\ \boldsymbol{H}^{11} \\ \boldsymbol{H}^{12} \end{pmatrix}, \tag{13}$$

where $\boldsymbol{I}$ is the identity matrix. Equation (13) can be efficiently solved for the components of the total correlation function in terms of the direct correlation function using a lower triangular-upper triangular (LU)-decomposition based equation solver.[23]

Equations (11) and (13) can now be solved iteratively, but one must bear in mind that given the Coulombic character of the interaction, the direct correlation functions are long ranged and their Fourier transforms must be handled with some care. One can renormalize the equations in terms of short ranged functions, along the lines of Refs. 18 and 19. Here, for simplicity we follow Lado's recipe[24,25] that retains

the formal structure of the ROZ equations in the Fourier space and only implies a minor reformulation of the closure. We then define long-range components of the interaction potentials as

$$\beta\phi_{ij}^{LR}(r) = z_i z_j \mathrm{erf}(r)/r,$$
$$\beta\tilde{\phi}_{ij}^{LR}(k) = 2\pi z_i z_j (1 - \mathrm{erf}(k/2)/k), \tag{14}$$

where i and j can either be $+$, $-$, or m_+, and erf denotes the error function. With these expressions, one can define a new set of short ranged correlations and short ranged interactions of the form

$$\beta\phi_{ij}^{SR}(r) = \beta V_{ij}(r) - \beta\phi_{ij}^{LR}(r), \tag{15}$$

$$c_{ij}^{SR}(r) = c_{ij}(r) + \beta\phi_{ij}^{LR}(r), \tag{16}$$

$$\gamma_{ij}^{SR}(r) = \gamma_{ij}(r) - \beta\phi_{ij}^{LR}(r), \tag{17}$$

with $\gamma_{ij}=h_{ij}-c_{ij}$ as usual. In this way the closure relation (11) can be rewritten into

$$c_{ij}^{SR}(r) = \exp[-\beta\phi_{ij}^{SR}(r) + \gamma_{ij}^{SR}(r)] - 1 - \gamma_{ij}^{SR}(r), \tag{18}$$

with only short range functions involved. Thus, the numerical Fourier transforms (either forward or backward) are only performed on short ranged functions, and the complete functions are recovered by adding or subtracting where appropriate the analytic Fourier transforms $\beta\tilde{\phi}_{ij}^{LR}(k)$. We note in passing that the functions involving correlations with the template (i.e., the m_- component) or between replicas are short ranged.

B. ROZ thermodynamics

Once the correlation functions are determined, we can calculate thermodynamic properties for the adsorbed fluid. A first quantity that can be evaluated is the excess internal energy per adsorbate particle,

$$\beta U/N = \frac{1}{2}\sum_{\alpha\nu}\frac{\rho_\alpha\rho_\nu}{\rho}2\pi\int drrh_{\alpha\nu}(r)\beta V_{\alpha\nu}^{\mathrm{Coul}}(r) + \sum_{\alpha}\frac{\rho_\alpha\rho_{m_+}}{\rho}2\pi\int drrh_{\alpha m_+}(r)\beta V_{\alpha m_+}^{\mathrm{Coul}}(r), \tag{19}$$

where the superscript Coul denotes the Coulombic part of the interaction and $\rho=\rho_+ + \rho_-$. In order to fully account for the interaction of the particles with the neutralizing background (which extends inside the cores of the matrix particles), $V_{\alpha m_+}^{\mathrm{Coul}}(r)$ is assumed to be nonzero all the way down to $r=0$, which only affects the value of the second integral in the right hand side of Eq. (19).

The virial equation for partly quenched systems is somewhat involved to evaluate;[26,27] however, the isothermal compressibility can easily be determined via[26]

$$\beta\frac{\partial P}{\partial\rho} = 1 - \sum_{\alpha,\nu}\frac{\rho_\alpha\rho_\nu}{\rho}2\pi\int drr(c_{\alpha\nu}^{SR}(r) - c_{\alpha\nu}^{r}(r)). \tag{20}$$

Finally, the ROZ-HNC direct expression for the chemical potential is[19,28,29]

$$\beta\mu_\alpha = -\sum_{i=+,-}\rho_{m_i}\tilde{c}_{m_i\alpha}^{R}(0) - \sum_{\nu=+,-}\rho_\alpha(\tilde{c}_{\nu\alpha}^{SR}(0) - \tilde{c}_{\nu\alpha}^{r}(0)) + \frac{1}{2}\sum_{i=+,-}\rho_{m_i}\int d\mathbf{r}h_{m_i\alpha}(r)\gamma_{m_i\alpha}(r) + \frac{1}{2}\sum_{\nu=+,-}\rho_\nu\int d\mathbf{r}(h_{\nu\alpha}(r)\gamma_{\nu\alpha}(r) - h_{\nu\alpha}^{r}(r)\gamma_{\nu\alpha}^{r}(r)) + \log(\rho_\alpha\Lambda_\alpha^2), \tag{21}$$

where Λ_α is the de Broglie wavelength for the α fluid particles, and in the first term of Eq. (21),

$$c_{m_i\alpha}^{R}(r) = c_{m_i\alpha}(r) + \beta V_{m_i\alpha}^{\mathrm{Coul}}(r) \tag{22}$$

in order to account for the background contribution[14] and remove the divergence at $k=0$. This quantity can be rewritten in terms of our short ranged functions as

$$\tilde{c}_{m_i\alpha}^{R}(0) = \tilde{c}_{m_i\alpha}^{SR}(0) + 2\sqrt{\pi}z_{m_i}z_\alpha\Gamma. \tag{23}$$

C. Porosity in the ROZ-HNC approximation

The porosity is a key quantity to describe the structure of a porous material. Here, and in accordance with literature,[30] we define the porosity as the fractional volume available to a single HS adsorbate of diameter, σ_t, in the material once the template has been removed. From the point of view of the simulation, the porosity can be estimated performing insertion attempts of a test particle in the matrix and evaluating the ratio between the accepted and rejected insertion attempts. Porosities calculated in this way agree well with those obtained from high temperature helium adsorption.[5,31] On the other hand, from the theoretical standpoint, a family of the Kirkwood–Salsburg-like hierarchy of integrals can also be used to define the porosity,[32]

$$\Phi(\rho_{m_+},\rho_{m_-}) = 1 + \sum_{s=1}^{\infty}\frac{\rho_{m_+}^{s}}{s!}\int d\boldsymbol{r}_2,\ldots,d\boldsymbol{r}_{s+1}f_{01}(\boldsymbol{r}_1,\boldsymbol{r}_2),\ldots, f_{01}(\boldsymbol{r}_1,\boldsymbol{r}_{s+1})g_{00}^{(s)}(\boldsymbol{r}_2,\ldots,\boldsymbol{r}_s+1;\rho_{m_+},\rho_{m_-}), \tag{24}$$

where $g_{00}^{(s)}$ is the sth order distribution function between matrix particles and f_{01} is the matrix-adsorbate Mayer function. Obviously, the porosity is an explicit function of the matrix density, ρ_{m_+}, and indirectly it also depends on the template density, ρ_{m_-}, through $g_{00}^{(s)}$. This latter quantity is conditioned by ρ_{m_-}, before quenching and removal of the template. Now, the simplest approximation for the porosity implies the neglect of the matrix particle correlations, by which one gets

$$\Phi(\rho_{m_+}) = \exp\left(\rho_{m_+}\int d\boldsymbol{r}f_{01}(r)\right), \tag{25}$$

which in our two-dimensional case reduces to

$$\Phi(\rho_{m_+}) = \exp[-\pi\rho_{m_+}(\sigma_{m_+} + \sigma_+)^2/16], \tag{26}$$

which obviously does not depend either on the matrix or on the template configuration. Only for very dilute matrices will this approximation be of any use. Van Tassel[30] introduced a

new integral equation to go beyond this simple approach. However, once the ROZ equations have been solved for a given system, a more practical alternative can be formulated based on the ROZ-HNC determination of the chemical potential. Following Zhang and Van Tassel,[9] one can split the net chemical potential of the adsorbate particle, α, into

$$\beta\mu_\alpha = \log(\rho_\alpha \Lambda_\alpha^2) - \log \Phi_\alpha + \beta\mu_\alpha^{\mathrm{ex}}(\rho_\alpha), \tag{27}$$

where Φ_α is the porosity of the material with respect to the component α and μ_α^{ex} is the excess part of the chemical potential solely due to the adsorbate α. According to Zhang and Van Tassel,[9] this quantity can be estimated by thermodynamic integration of the isothermal compressibility of the adsorbate, which in turn can be evaluated via Eq. (20). However, in the ROZ-HNC approximation, an alternative path emerges from a close examination of Eq. (21). Here one can easily separate those terms that stem solely from fluid-fluid (or fluid-replica and replica-replica) correlations from those that involve the matrix. The former are those that enter μ_α^{ex}, by which one can finally obtain for the porosity

$$\log \Phi_\alpha(\rho_{m_+}, \rho_{m_-}) = \sum_{i=+,-} \rho_{m_i} \tilde{c}^R_{m_i\alpha}(0) - \frac{1}{2} \sum_{i=+,-} \rho_{m_i} \int d\mathbf{r} h_{m_i\alpha}(r) \gamma_{m_i\alpha}(r). \tag{28}$$

Now, since the porosity is measured with respect to an uncharged test particle, the ROZ-HNC calculations will have to be carried out with $\rho_\alpha \to 0$ and in the limit of $T \to \infty$ (or $z_\alpha = 0$).

III. SIMULATIONS

In a first stage matrix configurations were obtained by performing canonical ensemble MC simulations at temperature T_m for a neutral two-component mixture (the matrix precursor components) of N_{m_+} charged HSs of diameter σ_{m_+} and charge z_{m_+} and N_{m_-} particles (the template) of diameter σ_{m_-} and charge z_{m_-}, satisfying charge neutrality, i.e., $N_{m_+} z_{m_+} + N_{m_-} z_{m_-} = 0$. The centers of mass of the particles are constrained to lie in a plane. Equilibrium configurations at several "time" intervals separated by $\approx 10^6$ MC moves per particle were frozen and the negative ions (template) removed. A neutralizing uniform background penetrating the matrix particles is assumed to restore charge neutrality. The numbers of matrix particles (positive ions) were typically $N_{m_+} = 80$ and 180 and the area A of the system was fixed by the target matrix density $\rho_{m_+} = N_{m_+}/A$. Matrix configurations were generated at the two temperatures $T_m^* = 1$ and $T_m^* = \infty$. The latter case amounts to simulate an uncharged HS mixture (though after the quench the matrix particles bear a charge z_{m_+}). In addition we considered a nontemplated matrix consisting of a quenched equilibrium configuration of a one component (uncharged) HS system at density ρ_{m_+} and diameter σ_{m_+}.

GCMC simulations[33] were then performed at fixed temperature T and total chemical potential μ for the matrix-adsorbate system consisting of a neutral mixture of positive and negative ions in the fixed matrix. The simulation steps consisted in performing, in a random way, displacement of an ion, insertion, or deletion of a neutral ionic cluster (pair of a positive and a negative ion for a 1:1 electrolyte, triplet of a positive ion and two negative ions in the case of a 1:2 electrolyte). Insertion and deletion steps used a biasing scheme preferentially sampling short interionic distances similar to the one proposed in Ref. 34 for bulk ionic fluids.

Ewald sums were applied to handle the Coulomb interactions between the different ionic species. The relevant expressions for the energy of the system and computational details are given in Ref. 35. For a given matrix, thermodynamic and structural properties of the annealed ionic fluid were averaged over 2×10^9 elementary moves after equilibration of the system. To assess the dependence of the results on matrix configuration, averages were further taken over three to four matrix realizations at selected state points. This dependence was largest in the case of the $T_m^* = \infty$ template matrix where the arrangement of the matrix particles is more inhomogeneous than, for instance, in the $T_m^* = 1$ case, but did not exceed 5% for the density at the lowest temperatures considered. For the matrix realizations at $T_m^* = 1$ the changes were much smaller and we contented ourselves to consider only a single matrix configuration.

An estimate of the partial excess chemical potentials μ_α^{ex} of the two ionic components was attempted by randomly inserting either a positive or negative test ion into the system. According to Widom's expression[36] the excess chemical potential of species α is given by

$$\mu_\alpha^{\mathrm{ex}} = -kT \ln\langle \exp(-\beta \Delta E_\alpha) \rangle, \tag{29}$$

where ΔE_α is the energy change in insertion of the test particle of species α and the brackets denote an average over a sufficiently large number of insertions. Note that ΔE_α includes the interaction energy of the inserted ion of charge z_i with the matrix background given by[37]

$$E_{bg}/kT = -z_i z_{m_+} N_{m_+} \frac{e^2}{kT} \frac{2\sqrt{\pi}}{\eta L^2}, \tag{30}$$

where η is the parameter which governs the rate of convergence of the real- and reciprocal-space contributions in the Ewald sum[35] and L is the box dimension. The total (ideal plus excess) chemical potential is then given by $\mu_\alpha = kT \ln(\bar{\rho}_\alpha) + \mu_\alpha^{\mathrm{ex}}$, where $\bar{\rho}_\alpha$ is the average density of ion α (the temperature dependent part of the ideal chemical potential is omitted). The method failed at low (negative) values of the total chemical potential, μ, due to insufficient statistics in our calculations. A possible source of error may also arise from the inability of the electroneutral system to properly screen the additional test charge.[38] Nonetheless, for a large number of state points, the chemical potentials calculated in this way added up correctly to the total (ideal plus excess) chemical potential (input value in the GCMC simulations) $\mu = \nu_- \mu_- + \nu_+ \mu_+$ (where $\nu_\pm$ are the stoichiometric coefficients of the electrolyte, which are conditioned by the electroneutrality constraint) and compared favorably with the integral equation predictions.

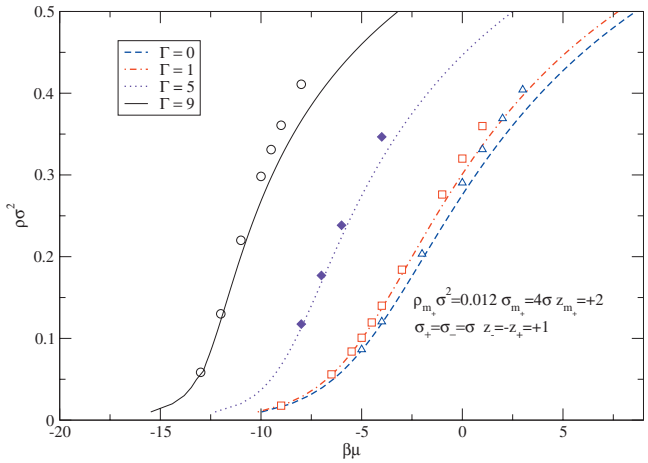

FIG. 1. Adsorption isotherms for a symmetric electrolyte in a dilute charged matrix (matrix A) at various inverse temperatures, $\Gamma = 1/T^*$. Symbols denote MC data and curves correspond to ROZ-HNC results.

IV. RESULTS

The integral equation has been solved following the procedure outlined in Sec. II, using a grid of 1500 points in r- and k-spaces, with the points in the k-space defined according to Lado's recipe.[21] The unequal grid spacing is such that the number of grid points to define the smallest core size (σ) is 100. We have carried out explicit calculations for two main types of matrices: model A matrix is obtained from quenching an asymmetric HS electrolyte, with charges $z_{m_+}=+2$ and $z_{m_-}=-1$, diameters $\sigma_{m_+}=4\sigma$ and $\sigma_{m_-}=\sigma$, and densities $\rho_{m_+}\sigma^2=0.012$, $\rho_{m_-}\sigma^2=0.024$. With this matrix, we have studied the adsorption of a 1:1 symmetric electrolyte (HSs of diameter σ) at various reduced temperatures. Since the matrix is diluted the results are essentially independent of the quenching temperature (we have considered $T_m^*=1$, $T_m^*=\infty$, and a plain HS matrix of $\sigma_{m_+}=4\sigma$ at $\rho_{m_+}\sigma^2=0.012$). The adsorption isotherms depicted in Fig. 1 correspond to matrix A obtained by quenching at $T_m^*=1$, and are indistinguishable from those obtained for $T_m^*=\infty$, or even for the HS matrix configuration with the same density and particle size. Note that the net chemical potential quantity is directly related to the mean activity, $\gamma_\pm$, coefficient through

$$\ln \gamma_\pm = \frac{1}{z_+ - z_-}\mu.$$

Figure 1 illustrates the strong dependence of the adsorption process on the fluid temperature, the load of the matrix being much higher as the fluid temperature is lowered. The performance of the ROZ-HNC equation is satisfactory.

A more detailed study has been performed on a second matrix model, denser and with larger charges. This model, denoted by matrix B, is obtained by quenching an asymmetric electrolyte composed of HSs of charge $z_{m_+}=+4$ and $z_{m_-}=-1$, diameters $\sigma_{m_+}=2\sigma$ and $\sigma_{m_-}=\sigma$, and densities $\rho_{m_+}\sigma^2=0.09$, $\rho_{m_-}\sigma^2=0.36$. We note in passing that these model parameters are not intended to explicitly represent a particular experimental system. They simply reflect general characteristics to be expected for an electrolyte confined in a real PILC: pillars with a substantial positive charge, larger than

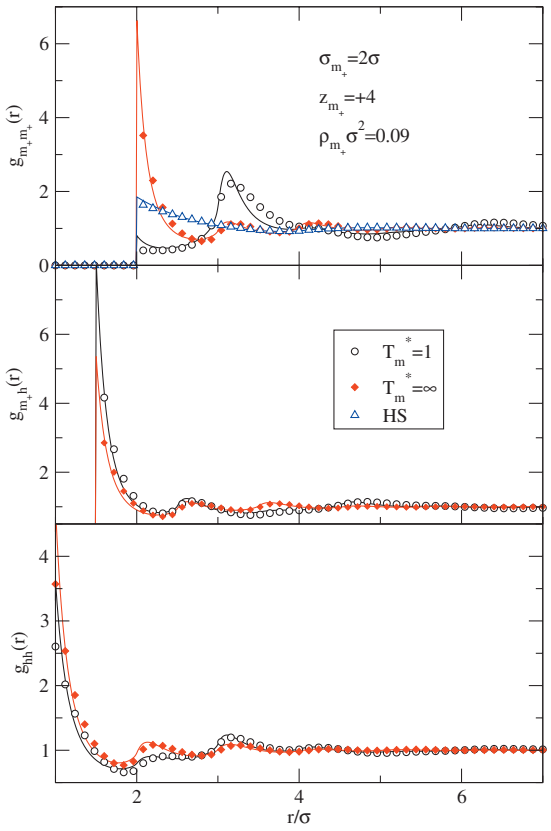

FIG. 2. Pair correlation functions of the matrix particles in model B (dense matrix). The correlation functions with a subscript h denote correlations involving the holes left by the template particles after their removal. Symbols represent simulation results and solid curves denote the HNC calculations.

that of the adsorbate ions, and pillar diameters also bigger than the adsorbate molecular sizes. The particular choice of parameters aims at generating a variety of matrix models and thermodynamic conditions that best illustrate the effects of pillar configuration and/or charge on the adsorption properties of simple electrolytes. A direct comparison with experimental systems is beyond the scope of this work.

The pair distribution functions of matrix model B for the quenching temperatures $T_m^*=1$, $T_m^*=\infty$ and the corresponding HS matrix ($\rho_{m_+}\sigma^2=0.09$ and $\sigma_{m_+}=2\sigma$) are depicted in Fig. 2. Now we observe a strong dependence of the matrix-matrix distribution function on the preparation procedure. On the other hand, "matrix-hole" and "hole-hole" (by hole we denote the position occupied by the template particle prior to its removal) are fairly similar. Figure 2 also illustrates the good performance of the HNC approach for the annealed asymmetric two-dimensional electrolyte. Snapshots of configurations for each type of matrix of model B are presented in Fig. 3.

The different porosities of each matrix model is already visible in the figure. As mentioned before, porosities can be explicitly calculated with respect to particles of diameter σ_t, using MC insertion tests or using the procedure outlined in Sec. II C. The corresponding values for the three types of model B matrices are collected in Table I. The ROZ-HNC reproduces almost quantitatively the MC values. On the other hand the simple second virial coefficient approach of

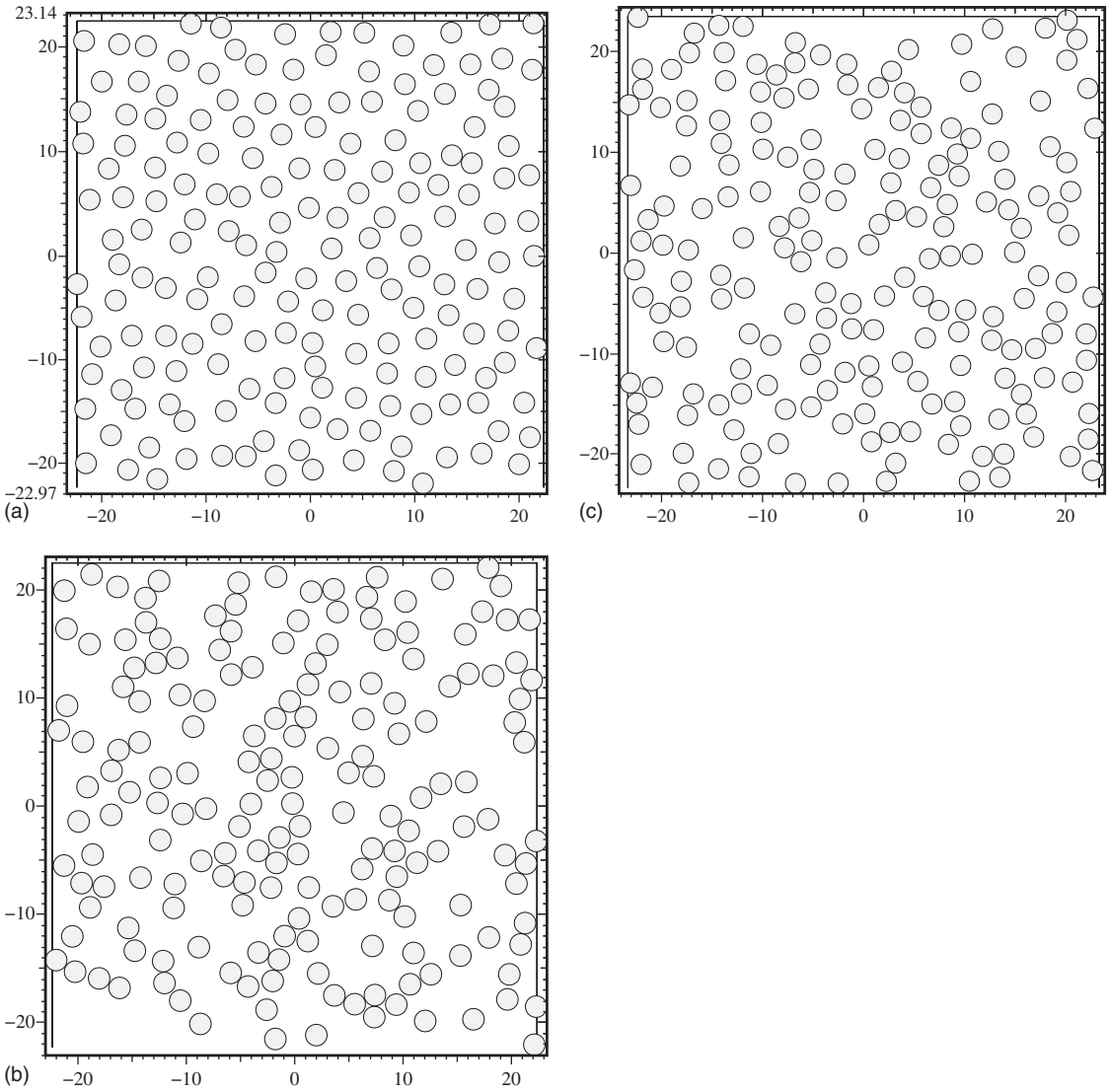

FIG. 3. Snapshots of model B matrices ($z_{m_+}=+4$, $\sigma_{m_+}=2\sigma$, and $\rho_{m_+}\sigma^2=0.09$) at $T_m^*=1$ (a), $T_m^*=\infty$ (b), and the corresponding plain HS system (c).

Eq. (26) only captures the decrease in the porosity when the test particle diameter increases from σ to 1.4σ, overestimating by far the porosity values. Interestingly the matrix with the larger porosity is obtained from the high temperature quench, $T_m^*=\infty$. This configuration corresponds to that of a HS mixture ($\sigma_{m_+}/\sigma_{m_-}=2$ and $\rho_{m_+}/\rho_{m_-}=1/4$) in which the m_- particles have been removed. In contrast the HS matrix (denoted in what follows by HS) corresponds to HSs of diameter σ_{m_+} at a density ρ_{m_+}. The removal of the template leaves a more open structure.[9] When the original matrix is charged, the arrangement of positive ions, more or less uniformly surrounded by their counterions, leads to a more regular distribution of matrix particles once the system is quenched and the template anions are removed. When the test particle is bigger, the larger amount of available volume of the $T_m^*=\infty$ matrix becomes more evident. It is found that its porosity is 50% higher than that of the $T_m^*=1$ matrix when $\sigma_t=1.4\sigma$, whereas this ratio goes down to 18% when $\sigma_t=\sigma$.

We now look at the fluid structure inside the porous matrix. The simplest case is a symmetric charged HS adsorbate, for which the ion-ion and matrix-ion correlations are depicted in Fig. 4 at low temperature for $T_m^*=1$. Once more

TABLE I. Matrix porosities for model B matrices with respect to HS test particles of diameter σ_t, calculated from MC insertion tests, in the ROZ-HNC approximation and neglecting matrix correlations [Eq. (26)].

	$\sigma_t=\sigma$			$\sigma_t=1.4\sigma$		
Model	MC	ROZ-HNC	Equation (26)	MC	ROZ-HNC	Equation (26)
$T_m^*=1$	0.381(5)	0.37	0.85	0.240(5)	0.21	0.81
$T_m^*=\infty$	0.441(1)	0.44	0.85	0.340(3)	0.34	0.81
No template	0.420(4)	0.40	0.85	0.310(6)	0.29	0.81

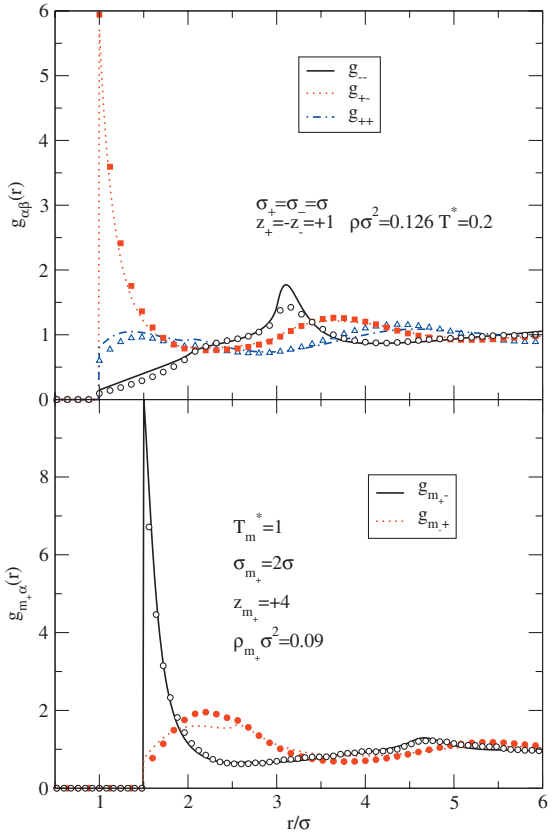

FIG. 4. Low temperature ($T^*=0.2$) ion-ion and matrix-ion pair correlation functions for the 1:1 electrolyte adsorbed in a model B (dense) matrix quenched at $T_m^*=1$. Symbols represent simulation results and solid curves denote the ROZ-HNC calculations.

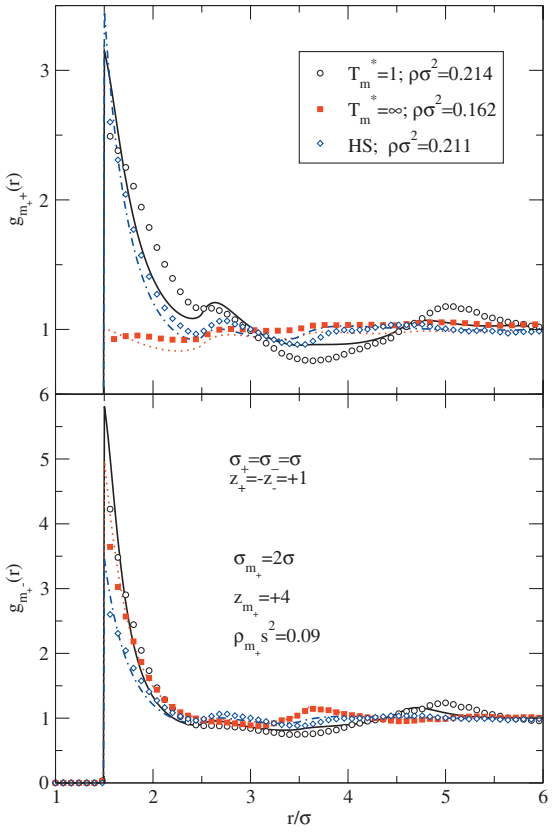

FIG. 5. Symmetric 1:1 electrolyte matrix-ion correlations at $T^*=1$ for the three matrices represented in Fig. 3. Parameters defining the adsorbate and the matrix are shown on the figure. Symbols represent simulation results and solid curves denote the ROZ-HNC calculations.

the ROZ-HNC performs reasonably well in this instance. Taking into account that we are now considering a symmetric electrolyte, the most noteworthy feature in this figure is the lack of symmetry between ++ and −− correlations. As a result of the presence of the matrix, there is a large exclusion sphere around negative ions, to the point that their first coordination sphere is centered around 3σ. Negative ions are attracted by the matrix particles and these are the source of the exclusion sphere. Additionally, cation-cation correlations are almost ideal (except for the core exclusion) and g_{++} hardly deviates from unity. Both ion-ion and matrix-ion correlations are dominated by the large charge and size of the matrix particles.

Now, we can compare the correlations for various matrix configurations. We first focus on the symmetric electrolyte at a somewhat higher temperature and density than those of Fig. 4. The corresponding matrix-ion correlations are depicted in Fig. 5. The largest difference in the correlations for the three types of matrix under consideration is seen in $g_{m_+ +}$, which is practically flat in the case of the $T_m^*=\infty$ matrix. The matrix-anion correlations are so strong that the matrix particles are fully screened by anions. Due to this, cations and matrix particle positions are practically uncorrelated (except for core exclusion) when the matrix is obtained by a high temperature quench. This is not the case when the matrix is formed by plain HSs (there is no matrix particle screening then) or from a low temperature quench ($T_m^*=1$). The matrix-fluid structure in this latter instance is much closer to what one would find in an annealed fluid, and the anions will try to fill in the voids left by the negative template particles. As to the performance of the ROZ-HNC, it turns out to be worse for $T_m^*=\infty$ matrix. In this case the Stillinger–Lovett screening conditions are largely violated (the positional correlation between matrix particles is not influenced by the charges), which is not the situation in the $T_m^*=1$ case. Note, however, that the net charge neutrality is preserved by the negative background that ideally accounts for the negative charge distribution in the original layers of the intercalated clay.

If we now focus on the ion-ion correlations (see Fig. 6, now for the fully asymmetric 1:2 electrolyte), it is again the $T_m^*=\infty$ matrix that most influences the fluid correlations, in particular, the ++ distribution function. It is also in this case that the ROZ-HNC performs worse. We see that again, as in Fig. 4, the anion-anion distribution function exhibits very little structure except for a maximum at 3σ and a large correlation hole between 0 and 2σ that are both determined by the anion-matrix-anion correlations. In contrast the ++ correlations are considerably enhanced near contact, and the smooth maximum at 1.5σ in Fig. 4 develops into a well defined HS like maximum at σ in Fig. 6. This is in part due to the fact the ++ repulsion is less pronounced at the higher temperature of Fig. 6 ($T^*=1$ versus $T^*=0.2$ in Fig. 4). As mentioned, the ++ correlations are mostly influenced by the presence of the $T_m^*=\infty$ matrix particles, and it thus turns out that fluid cations cluster together, to a larger extent in this case. This also most likely stem from violation of the screen-

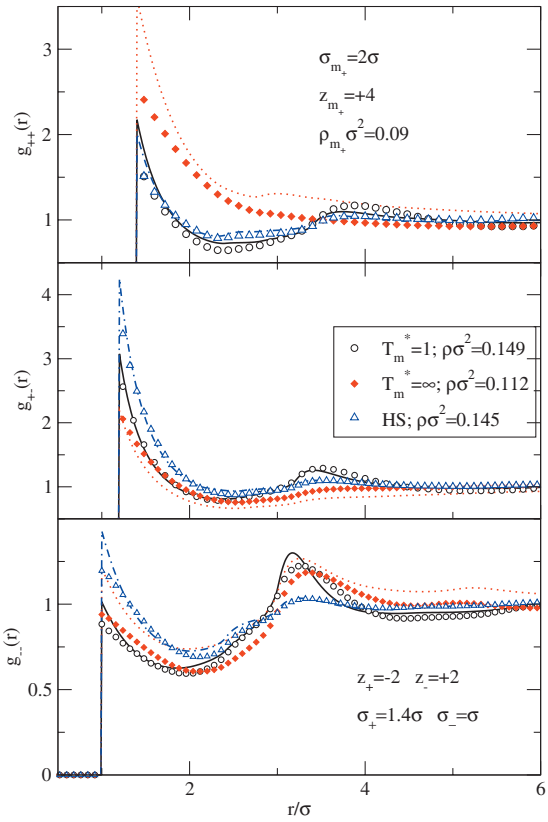

FIG. 6. Asymmetric electrolyte ion-ion correlations for the three matrices represented in Fig. 3 at $T^*=1$. Parameters defining the adsorbate and the matrix are shown on the figure. Symbols represent simulation results and solid curves denote the ROZ-HNC calculations.

ing conditions (of the fluid correlation functions) at a local scale induced by the positively charged matrix particles. This feature is further enhanced as the temperature is lowered (see Fig. 7), and in fact it might be at the root of the breakdown of the ROZ-HNC integral equation when the temperature is

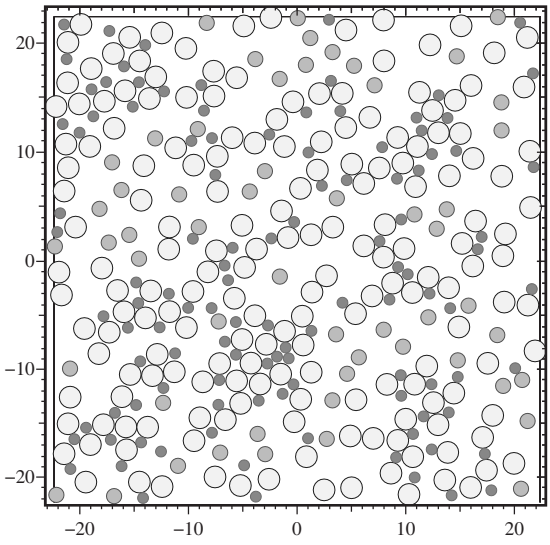

FIG. 7. Snapshot of a configuration of the 1:2 electrolyte ($\rho\sigma^2=0.0814$) adsorbed in the model B matrix (high temperature quench, $T_m^*=\infty$) at low temperature, $T^*=0.2$. Matrix particles are denoted by the large light gray disks. Fluid anions are the smallest (black) disks and fluid cations are represented by the medium sized gray disks. The local segregation of cations and anions induced by the charged matrix particles is clearly visible.

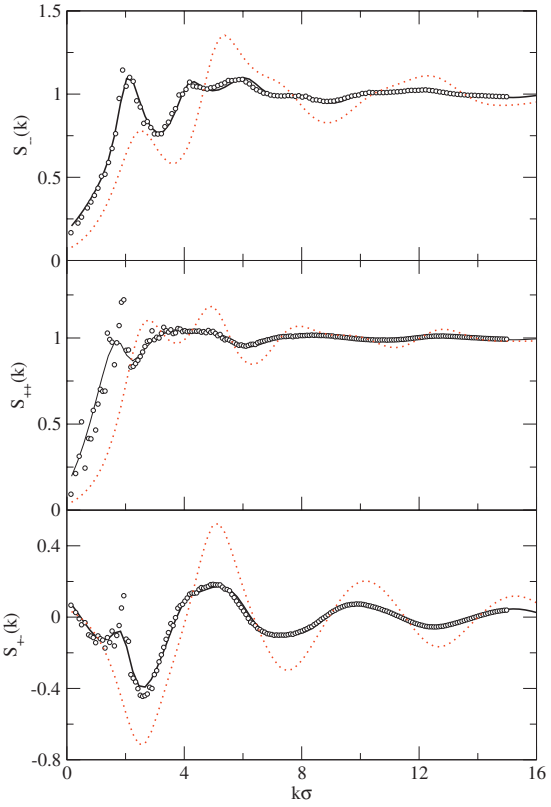

FIG. 8. Ion-ion structure factor asymmetric 1:2 electrolyte adsorbed in model B matrix configuration from a quench at $T_m^*=1$. The fluid density is $\rho\sigma^2=0.2169$ and $T^*=1$. Symbols represent simulation results and the solid curve denotes the ROZ-HNC calculations. Bulk results obtained in the HNC for the same chemical potential as that of the adsorbed fluid in the GCMC calculations are shown as a dashed curve for comparison.

lowered beyond a certain threshold ($T^*=0.4$ for low densities when $T_m^*=\infty$). This breakdown might well be interpreted as a signature of a local phase segregation.

In close connection with the ion-ion pair distribution functions, in Fig. 8 we plot the partial structure factors defined as

$$S_{\alpha\nu}(k) = \delta_{\alpha\nu} + \sqrt{\rho_\alpha \rho_\beta}\,\tilde{h}_{\alpha\nu}(k). \tag{31}$$

In the figure, one sees how the ROZ-HNC reproduces well the simulated data. Also, for comparison we plot the partial structure factors of the bulk electrolyte calculated in the HNC approximation at the same net chemical potential as the adsorbed fluid. Essentially, the bulk and adsorbed fluid structure factors exhibit the same features with the maxima and minima shifted in the latter instance to somewhat lower values. This shift is likely due to the effect of the matrix particles that mediate between ion-ion correlations and, as seen in Fig. 6, induce an increase in the radii of the coordination shells with respect to what one would find in their absence.

Another interesting correlation that deserves to be investigated concerns the ion-hole distribution function. In those matrices obtained from a templating process, we can evaluate the correlations between the adsorbed fluid ions and the positions originally occupied by the negative template particles. This hole-ion distribution functions are plotted in Fig. 9 for the fully symmetric 1:1 electrolyte and the asymmetric 1:2 electrolyte. Obviously only the templated matrices are

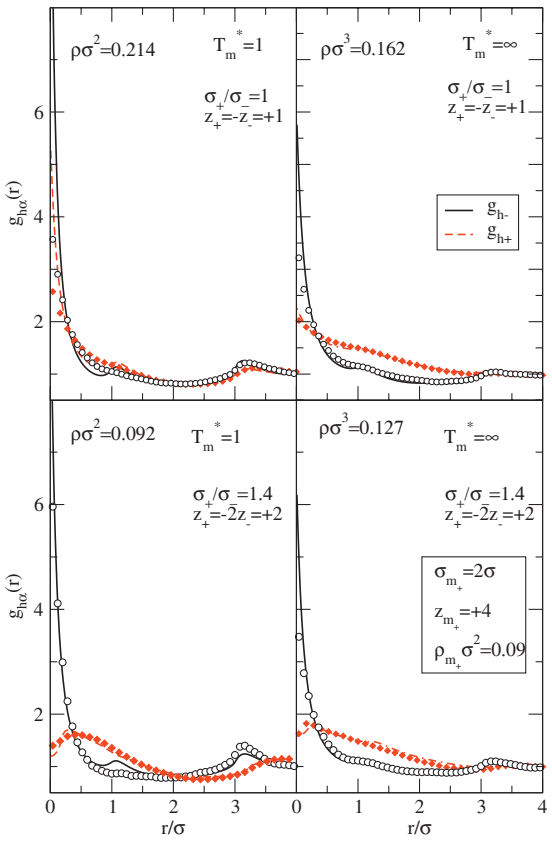

FIG. 9. Ion-hole matrix correlations for the fully symmetric 1:1 electrolyte (upper graphs) and asymmetric electrolyte (lower graphs) adsorbed in matrix configurations from quenches at $T_m^*=1$ and $T_m^*=\infty$. Parameters defining the adsorbate and the matrix are shown in the figure. Symbols represent simulation results and solid curves denote the ROZ-HNC calculations.

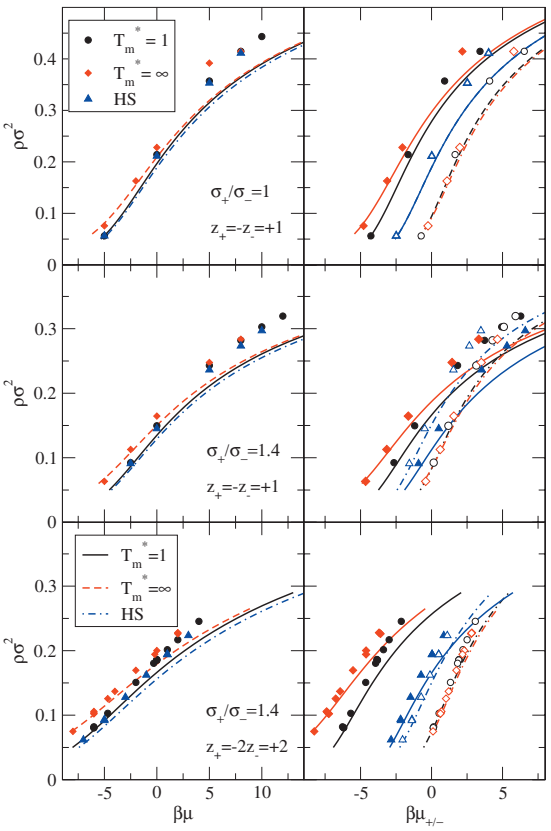

FIG. 10. On the left graphs, full adsorption isotherms for the fully symmetric 1:1 electrolyte (upper graphs), the asymmetric 1:1 electrolyte (middle graph), and the asymmetric 1:2 electrolytes (lower graph) adsorbed in matrix configurations from quenches at $T_m^*=1$ and $T_m^*=\infty$ and a plain HS matrix. On the right graphs the adsorption isotherms for fluid cations (filled symbols and solid curves) and anions (empty symbols and dashed-dotted curves) are depicted. Symbols represent simulation results and curves denote the ROZ-HNC calculations.

considered in this analysis. At first sight, one observes a larger tendency of the anions to occupy the holes left in the matrix by the template. This is particularly well understood for the $T_m^*=1$ matrix since in this case the original quench before the template removal was an equilibrium configuration (i.e., minimum energy), and it is understandable that the system tries to reproduce such a minimum energy configuration filling again the cavities with anions. The results are qualitatively similar for symmetric and asymmetric electrolytes, except that the hole-cation correlation shows a slight depletion at $r=0$, which is likely the result of the size mismatch between the adsorbed cation and the templated particles. As to the ROZ-HNC performance for these quantities it can be deemed reasonable, except when approaching $r=0$, where it largely overestimates the simulation results. This failure of the theory is connected with its intrinsic inability to fulfill the zero separation theorems, and it has also been observed in the penetrable sphere fluid.[39]

With all these structural information in mind, we can focus now on the adsorption isotherms, which are the most significant properties in our system. These are depicted for the three types of electrolyte and the three model B matrices under consideration in Fig. 10. Once more, we find the ROZ-HNC agrees reasonably well with the MC results. At high chemical potentials the adsorbate loads are underestimated (i.e., the chemical potential overestimated at a given fluid density), which is a direct consequence of the well-known HNC overestimation of virial pressures (or contact values in hard core systems) in simple fluids.[40] We note that these states have relatively large values of $\partial\beta P/\partial\rho$, indicating that despite the low absolute values of ρ the system corresponds to a fairly dense fluid. Both theory and simulation predict that the $T_m^*=\infty$ matrix allows for higher adsorbate loads, and that the plain HS matrix and the $T_m^*=1$ templated matrix lead to practically indistinguishable adsorption isotherms (notice however that the load of the HS matrix is slightly lower than that of the $T_m^*=1$ matrix for the same chemical potential, both in the ROZ-HNC and in MC results). The larger capability of the $T_m^*=\infty$ templated matrix as adsorbent is also made apparent by the porosity results shown in Table I. In contrast, according to the values of porosity, one should expect that the HS matrix should make possible a somewhat larger load than the $T_m^*=1$ templated matrix. The fact that the situation is reversed (both in MC and ROZ-HNC results) indicates that this effect is not geometric but due to the presence of charges in the adsorbate. It is anyhow somewhat striking that matrix configurations structurally speaking so different (see Fig. 2) lead to relatively similar adsorption curves. This is even more remarkable if one compares the fluid-matrix contribution to the internal (configurational) energy of the system, to the point that in the case of the HS matrix this contribution vanishes, whereas it amounts to

around 20%–30% of the total internal energy for the $T_m^*=1$ matrix at $T^*=1$ (and larger at lower temperatures). This large contribution is hardly noticeable in the net adsorption isotherms of Fig. 10 (which only exhibit significant differences in the $T_m^*=\infty$ case). This implies that for a given temperature, geometry (i.e., the porosity of the material) is the leading factor controlling adsorption, and the energetics play a secondary role.

Interestingly, if we now look at the individual cation and anion contributions to the chemical potential, shown on the right graphs in Fig. 10, the effect of each matrix type is more clearly distinguishable. In the case of the HS matrix, obviously $\mu_+=\mu_-$ when the electrolyte is symmetric. When the adsorbate symmetry is broken the equality of the chemical potentials disappears, and the ionic charge and size determine the sign and size of $\Delta\mu=\mu_+-\mu_-$. Perhaps the most interesting feature to be stressed in the μ_+ and μ_- curves is the relative insensitivity of μ_- with regard to the precise topology of the matrix (but not the charge) so that $T_m^*=1$ and $T_m^*=\infty$ results are hardly distinguishable. On the other hand, μ_+ is much more dependent on the matrix topology, and both HNC and simulation results exhibit clear differences. This is most likely due to the fact that the matrix itself is made of positively charged particles, so any configurational change will affect the work needed to insert a positive ion to a larger extent than a negative ion. The net adsorption isotherm is determined by the work of insertion of neutral clusters so this effect on μ_+ is also reflected on the net adsorption isotherm. As mentioned, it is somewhat remarkable that the HS matrix leads to net adsorption curves quite similar to those of the $T_m^*=1$ matrix, even if the μ_+ and μ_- curves are quite different. In this instance the matrix charge effects seem to cancel out, and as explained above only geometric effects (i.e., the porosity) are important.

In summary, we have presented a detailed study of the adsorption behavior of symmetric 1:1, size asymmetric 1:1, and fully asymmetric 1:2 electrolytes in two-dimensional templated matrices obtained by high and low temperature quenches of an asymmetric electrolyte with subsequent removal of the negative ions (in an attempt to devise an idealized model of a quasi-two-dimensional intercalated cationic clay) and compared them with adsorption in a plain uncharged HS matrix. The ROZ-HNC results agree reasonably well with the MC simulations as far as structure, porosities, and adsorption isotherms are concerned. The templated matrices obtained by high temperature quenches allow for higher adsorbate loads, especially at low chemical potentials (pressures) where energetic effects dominate over packing constraints. A natural extension of this work should account for interlayer separations larger than one molecular diameter, having a 3D inhomogeneous partly quenched medium. This problem could, in principle, be tackled following the approach of Pizio and Sokolowski[12] or Pérez *et al.*[13] Work on this is under way.

Also, one might easily extend the present approach to incorporate a molecular integral equation treatment, such as that of Fernaud *et al.*[17,41] by which the volumetric and calorimetric adsorption isotherms[42] of substances such as N_2, O_2, and other simple molecular and atomic gases and their mixtures can readily be calculated. This application would then be in close connection with the use of PILCs as molecular sieves for the separation of N_2 from air, a relevant problem from the experimental and applied standpoint.[43]

ACKNOWLEDGMENTS

E.L. gratefully acknowledges the support from the Dirección General de Investigación Científica y Técnica under Grant No. MAT2007-65711-C04-04 and from the Dirección General de Universidades e Investigación de la Comunidad de Madrid under Grant No. S0505/ESP/0299 and Program MOSSNOHO-CM.

[1] R. T. Yang and M. S. A. Baksh, AIChE J. **37**, 679 (1991).
[2] A. Corma, Chem. Rev. (Washington, D.C.) **97**, 2373 (1997).
[3] K. Ohtsuka, Chem. Mater. **9**, 2039 (1997).
[4] S. Cheng, Catal. Today **49**, 303 (1999).
[5] L. D. Gelb and K. E. Gubbins, Langmuir **15**, 305 (1999).
[6] L. D. Gelb, K. Gubbins, R. Radhakrishnan, and M. Sliwinska-Bartkowiak, Rep. Prog. Phys. **62**, 1573 (1999).
[7] W. G. Madden and E. D. Glandt, J. Stat. Phys. **51**, 537 (1988).
[8] J. A. Given and G. Stell, J. Chem. Phys. **97**, 4573 (1992).
[9] L. Zhang and P. R. van Tassel, J. Chem. Phys. **112**, 3006 (2000).
[10] S. L. Zhao, W. Dong, and Q. H. Liu, J. Chem. Phys. **125**, 244703 (2006).
[11] S. L. Zhao, W. Dong, and Q. H. Liu, J. Chem. Phys. **127**, 144701 (2007).
[12] O. Pizio and S. Sokolowski, Phys. Rev. E **56**, R63 (1997).
[13] L. Pérez, S. Sokolowski, and O. Pizio, J. Chem. Phys. **109**, 1147 (1998).
[14] M. Baus and J.-P. Hansen, Phys. Rep. **59**, 1 (1980).
[15] P. Debye and E. Hückel, Phys. Z. **24**, 185 (1923).
[16] D. Levesque, J. J. Weis, and G. N. Patey, J. Chem. Phys. **72**, 1887 (1980).
[17] M. J. Fernaud, E. Lomba, C. Martín, D. Levesque, and J.-J. Weis, J. Chem. Phys. **119**, 364 (2003).
[18] B. Hribar, V. Vlachy, A. Trokhymchuk, and O. Pizio, J. Phys. Chem. B **103**, 5361 (1999).
[19] B. Hribar, V. Vlachy, and O. Pizio, J. Phys. Chem. B **105**, 4727 (2001).
[20] M. Lukšič, B. Hribar-Lee, and V. Vlachy, J. Phys. Chem. B **111**, 5966 (2007).
[21] F. Lado, J. Comput. Phys. **8**, 417 (1971).
[22] J. D. Talman, J. Comput. Phys. **29**, 35 (1978).
[23] E. Anderson, Z. Bai, C. Bischof, S. Blackford, J. Demmel, J. Dongarra, J. Du Croz, A. Greenbaum, S. Hammarling, A. McKenney, and D. Sorensen, *LAPACK Users' Guide*, 3rd ed. (Society for Industrial and Applied Mathematics, Philadelphia, PA, 1999).
[24] F. Lado, Phys. Rev. B **17**, 2827 (1978).
[25] E. Lomba, J. J. Weis, and F. Lado, J. Chem. Phys. **127**, 074501 (2007).
[26] M. L. Rosinberg, G. Tarjus, and G. Stell, J. Chem. Phys. **100**, 5172 (1994).
[27] W. Dong, X. S. Chen, and W. M. Zheng, Phys. Rev. E **72**, 012201 (2005).
[28] L. L. Lee, J. Chem. Phys. **97**, 8606 (1992).
[29] M.-J. Fernaud, E. Lomba, and L. L. Lee, J. Chem. Phys. **111**, 10275 (1999).
[30] P. R. Van Tassel, Phys. Rev. E **60**, R25 (1999).
[31] A. L. Myers, J. A. Calles, and G. Calleja, Adsorption **3**, 107 (1996).
[32] G. Tarjus, P. Schaaf, and J. Talbot, J. Stat. Phys. **63**, 167 (1991).
[33] D. Frenkel and B. Smit, *Understanding Molecular Simulation* (Academic, London, 1996).
[34] G. Orkoulas and A. Z. Panagiotopoulos, J. Chem. Phys. **101**, 1452 (1994).
[35] J.-J. Weis, D. Levesque, and J. M. Caillol, J. Chem. Phys. **109**, 7486 (1998).
[36] B. Widom, J. Chem. Phys. **39**, 2808 (1963).
[37] J.-J. Weis, D. Levesque, and S. Jorge, Phys. Rev. B **63**, 045308 (2001).
[38] B. R. Svensson and C. E. Woodward, Mol. Phys. **64**, 247 (1988).
[39] M.-J. Fernaud, E. Lomba, and L. L. Lee, J. Chem. Phys. **112**, 810 (2000).

[40] J.-P. Hansen and I. McDonald, *Theory of Simple Liquids*, 2nd ed. (Academic, London, 1990).
[41] M. J. Fernaud, E. Lomba, and J.-J. Weis, Phys. Rev. E **64**, 051501 (2001).
[42] D. Nicholson and N. G. Parsonage, *Computer Simulation and the Statistical Mechanics of Adsorption* (Academic, London, 1982).
[43] R. T. Yang, *Gas Separation by Adsorption Processes* (Butterworths, Boston, 1987).